Hindawi
Advances in Civil Engineering
Volume 2020, Article ID 8833256, 13 pages
https://doi.org/10.1155/2020/8833256

Research Article

Mechanical Behavior and Calculation Method for RC Fifteen-Pile Cap of Mixed Passenger and Freight Railway Bridge

Hongmeng Huang,[1] **Lu Cui**,[2] **and Wei Lu**[1]

[1]*School of Civil Engineering, Northwest Minzu University, Lanzhou 730030, China*
[2]*Yantai Academy of Urban Construction and Design Co., Ltd., Yantai 264003, China*

Correspondence should be addressed to Hongmeng Huang; huanghongmeng_1987@163.com

Received 19 July 2020; Revised 13 August 2020; Accepted 21 August 2020; Published 18 September 2020

Academic Editor: Xueping Fan

The thickness, reinforcement, and concrete strength grade of railway caps in China are generally determined according to the force, yet the method for calculating the force is unclear. To date, there is no desirable calculation method for analyzing the caps. Based on the fifteen-pile thick cap of mixed passenger and freight railway, the influencing factors on cap bearing capacity were analyzed using finite element method (FEM). The variations of load-bearing capacity and mechanical behavior of thick cap were characterized by introducing rigid angle α. Results indicated that ultimate load-bearing value of the cap increased linearly with the increase of concrete strength grade, and an increasing load-bearing capacity of the reinforcement distributed in the pile diameter range was larger than that of the uniform reinforcement; when the reinforcement ratio was 0.15%, it increased by 9.3%. The cap showed punching failure when $\alpha < 45^{\circ}$. The reaction force at each pile top under vertical load was not equal; thereby, the cap was not absolutely rigid. The principal compressive stress trajectories in the concrete were distributed in the range of connecting the pile and the outer edge of the pier, and the effective tensile stresses in the reinforcement were mainly distributed in the diameter range of pile and pile connection, which is in accord with the stress mode of the ordinary spatial truss model. Based on this, a spatial truss model applicable to the design of railway caps is proposed, and a method for calculating reaction force at pile top and formulas for calculating the bearing capacity of strut and tie were presented. The feasibility of the proposed method was also verified by comparison with FEM results.

1. Introduction

The cap is an important component for transferring the upper load, and its internal forces are complex, which is especially the case for the forces of thick caps of group piles foundation. Many researchers have studied the factors affecting the bearing capacity and failure forms of caps. Guo [1] and Souza et al. [2], respectively, introduced punching-span ratio and shear span-depth ratio to distinguish the different failure forms of the caps. Huang et al. [3] analyzed the impact exerted on bearing capacity of pier and pile after increasing pile cap height by using the standard formula and numerical simulation method. Bloodworth et al. [4] studied the effects of shear span, cap width, and reinforcement ratio on the shear behavior of the cap under full-width wall loading, observed strut-and-tie model (STM), and thereby proposed an improved modified strut-and-tie method which gives more accurate predictions for the analysis of a four-pile cap.

STM is considered a commonly used method for the analysis and design of reinforced concrete structures [5], which was first introduced as an alternative approach for the design of pile caps and D-region members into the ACI 318-02 [6]. Based on ACI 318 [7] and BS 8110-1 [8], Chetchotisak and Teerawong [6] introduced the strength reduction factor as a safety index to ensure the safety of caps designed by STM method. Abdul-Razzaq and Farhood [9] designed and manufactured 12 RC cap specimens with different number of piles, comparatively studied the difference of bearing capacity and failure mechanism of the specimens designed according to the traditional section design method and the STM, and pointed out the shortcomings of cap design in ACI

318. Existing research on the application of STM mainly focused on the few pile caps, although STM was modified and improved by model tests and FEM, and a higher precision STM was proposed [2, 10–16]. In the literature, the compatibility and tensile contributions of concrete materials [2], modifying the node and tie parameters [14], the size effect (decreasing strength while increasing member size) [15], or the constitutive laws and strain compatibility of cracked reinforced concrete [10] were considered.

Most of the aforementioned research is based on few pile caps in the building structure. CAN/CSA S6-14 [17], JTG 3362-2018 [18], and AASHTO LRFD-2017 [19] all put forward STM applicable to the calculation of pile caps and made specific provisions on the calculation parameters of strut and tie. However, at present, there are few studies dealing with railway caps. In order to meet the requirements of bearing capacity and stiffness, thick cap and group piles foundation are mostly adopted in railway bridge. Mechanical characteristics of railway bridge caps are different from those of few pile caps in building structure. The thickness, reinforcement, and concrete strength grade of railway caps in China are generally determined according to the force; the pile cap is usually designed by controlling the rigid angle and setting steel bars mesh at the bottom [20]. Although this method has proved to be reliable in long-term engineering construction practices, it is unclear how the force was calculated. To date, there is no better calculation method for analyzing the caps. In this study, finite element method (FEM) was used to study the influencing factors of bearing capacity and mechanical behavior of caps based on the fifteen-pile thick cap of mixed passenger and freight railway. For more accurate mechanical characteristics of the cap, ANSYS software was used to establish the analytical model of the prototype cap. Moreover, by taking into account factors such as concrete strength grade, pile spacing, cap thickness, reinforcement ratio, reinforcement distributed form, load form, and their variations, this paper analyzed the influence of each factor on bearing capacity, failure mechanism inside the cap, stress trajectories in the concrete, stresses distribution in the reinforcement, and law of the reaction force at pile top. This study was seeking to determine whether STM method is suitable for the calculation of railway cap and proposed the calculation method of cap bearing capacity.

2. Establishment of Finite Element Analysis Model

A fifteen-pile cap of mixed passenger and freight railway contains two-floor caps. The plane dimension of the first-floor and second-floor cap is $18.6\,\text{m} \times 12.2\,\text{m}$ and $13.4\,\text{m} \times 7.0\,\text{m}$, respectively; the thickness of each floor cap is 3 m, and the concrete strength grade is C30. The cap is designed according to the reinforcement on six sides, with steel bars being evenly distributed orthogonally at its bottom. The steel bar grade is HRB335, with a diameter of 25 mm and a spacing of 10 cm, and the reinforcement ratio is 0.17%. The cap is connected with the bored pile with a diameter of 150 cm. The concrete strength grade of pile and pier is C30 and C35, respectively. The main dimensions of the cap and number of piles are shown in Figure 1.

According to the structural characteristics and calculation requirements of railway caps, the stress-strain relationship of concrete under uniaxial compression [Figure 2(a)] was referring to the curve specified in GB 50010-2010 (2015 edition) [21]. Concrete was simulated using SOLID65 3D solid element in ANSYS software, and the failure criterion was selected based on the five-parameter model of Willam–Warnke criterion.

SOLID65 can be used to calculate the cracking and crushing of concrete with the special cracking and crushing capabilities. Combined with the material characteristics of reinforced concrete, the shear transfer coefficients are introduced, and the uniaxial tensile strength f_t and uniaxial compressive strength f_c of concrete are added to simulate the cracking and crushing of concrete. In this paper, shear transfer coefficient for an open crack $\beta_t = 0.5$, shear transfer coefficient for a closed crack $\beta_c = 0.95$, uniaxial tensile strength f_t, and uniaxial compressive strength f_c were determined according to the concrete strength grade.

Constitutive relation of steel bar was simplified as uniaxial stress, and the ideal elastic-plastic model was adopted to ignore the stress strengthening stage [Figure 2(b)]. When constructing the finite element model, the steel bars were diffused in the concrete elements according to the volume ratio of reinforcement and the coordinate system, and the concrete element was regarded as a continuous uniform material without taking into consideration the bond and slip between steel bar and concrete.

The pile-soil interaction model adopted the linear elastic hypothesis and used spring to simulate soil stiffness [22]. That is to say, it took into consideration the lateral resistance of soil on the pile side and its distribution, the vertical resistance of soil, and the compression of pile itself. The constraint of soil on pile foundation was equivalent to a series of discontinuous springs which were simulated by spring element COMBIN14 in ANSYS software. Spring stiffness coefficient was calculated by the "m" method based on the linear elastic hypothesis. Figure 3 shows the finite element model.

3. Analysis of Influencing Factors on Cap

In order to analyze the effects of some factors such as concrete strength grade, pile spacing, cap thickness, bottom reinforcement ratio, reinforcement distributed form, and load form on the mechanical behavior of the cap, rigid angle α was introduced, which is defined as the angle of the extension of the outer edge of the pier root to the outer edge of the pile top. The change of pile spacing or cap thickness was considered as the change of α. The parameters of each influencing factor were changed according to Table 1, and other unchanged parameters can be seen in Figure 1. In Table 1, the concentrated reinforcement was within the pile diameter range. The combined load containing horizontal force, vertical force, and bending moment was considered by applying the seismic force at the pier bottom to the cap top through the seismic calculation of the bridge structure.

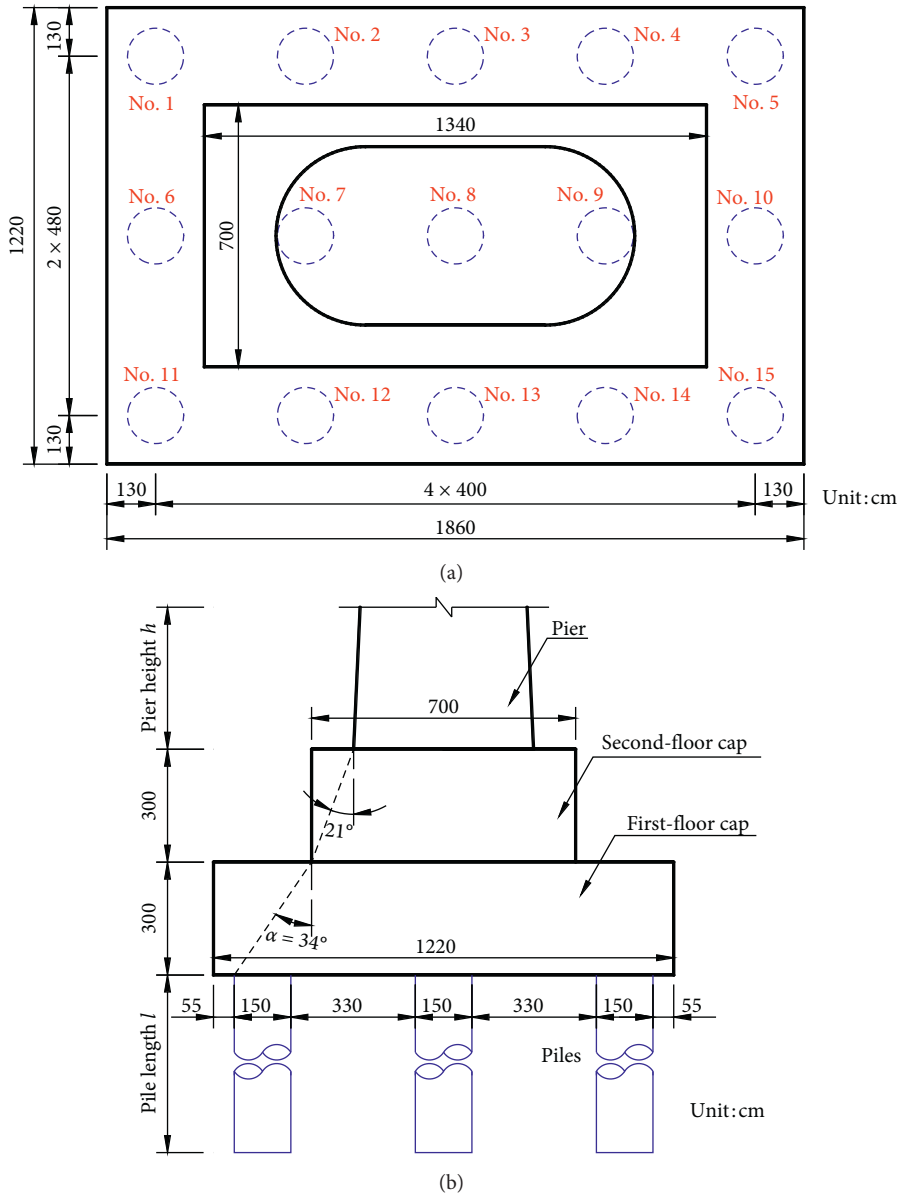

Figure 1: Main layout and section dimensions of pile and cap. (a) Plane dimensions and piles' number. (b) Elevation dimensions

3.1. Load-Bearing Capacity Analysis. The relationships of vertical ultimate load at cap top with concrete strength grade, pile spacing, cap thickness, and reinforcement ratio are shown in Figure 4. Vertical ultimate load at cap top with different reinforcement ratios and reinforcement distributed forms is shown in Table 2.

As can be seen from Figure 4 and Table 2, the ultimate load increased linearly with the increase of concrete strength grade. The ultimate load had its maximum when the longitudinal pile spacing was 4.8 m ($\alpha = 34^{\circ}$), and it decreased as spacing >4.8 m. The ultimate load showed an increasing trend with the increase of cap thickness, and its increasing tendency began to slow down as cap thickness >3.0 m. The ultimate load increased with the increase of the reinforcement ratio, and its increasing tendency began to slow down as reinforcement ratio >0.15%. When reinforcement ratio of the cap was 0.12% and 0.15%, the load-bearing capacity of the reinforcement distributed in the pile diameter range increased by 9.3% and 4.2% compared to that of the uniform reinforcement, respectively.

3.2. Failure Mechanism. When $\alpha = 26^{\circ}$ or $\alpha = 27^{\circ}$ [see Figure 5(a)], cracks first appeared around the pile, and they expanded upward as load increased, showing the fastest speed, around the middle pile. At cap bottom, radial cracks appeared along the line between the middle pile and other piles and developed continuously. Since the inside edge pile of No. 2 to No. 4 and No. 12 to No. 14 [see Figure 1(a)] shared the same vertical line with the edge of the second-floor cap, cracks developed vertically.

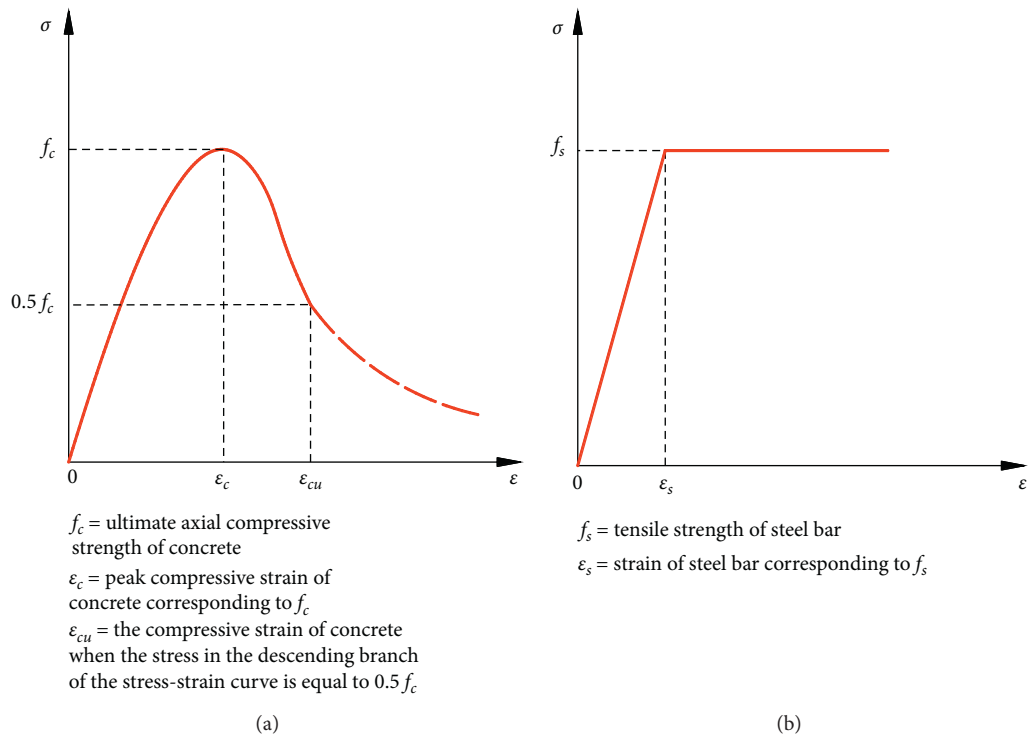

Figure 2: Stress-strain curve of materials. (a) Concrete under uniaxial compression. (b) Steel bar under monotonic tension.

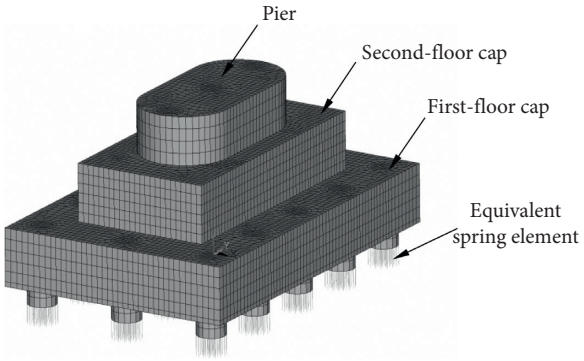

Figure 3: Finite element analysis model of pile cap.

Table 1: Parameter variation of influencing factors.

Influencing factors		Parameter variation
Concrete strength grade		C25, C30, C35, C40, C45
Longitudinal pile spacing		4.2 m ($\alpha = 26^\circ$), 4.8 m ($\alpha = 34^\circ$), 5.4 m ($\alpha = 41^\circ$), 6.0 m ($\alpha = 47^\circ$), 6.6 m ($\alpha = 52^\circ$)
First-floor cap thickness		2.0 m ($\alpha = 46^\circ$), 2.5 m ($\alpha = 39^\circ$), 3.0 m ($\alpha = 34^\circ$), 3.5 m ($\alpha = 30^\circ$), 4.0 m ($\alpha = 27^\circ$)
Reinforcement ratio	Uniform reinforcement	0.06%, 0.12%, 0.15%, 0.18%, 0.20%, 0.25%
	Concentrated reinforcement	12%, 0.15%
Load form		Vertical load, combined load

When $\alpha < 45^\circ$ [see Figures 5(b) and 5(c)], cracks first appeared at the inner edge of the edge pile and extended obliquely upward. As cracks extended to a certain height, they began to appear around the middle pile and spread obliquely to the top of the middle span. They then converged with the oblique cracks of No. 2 to No. 4 and No. 12 to No. 14 edge piles and spread obliquely towards cap top. Finally, they connected to the oblique cracks of other piles at cap top, declaring cap damage by showing punching failure.

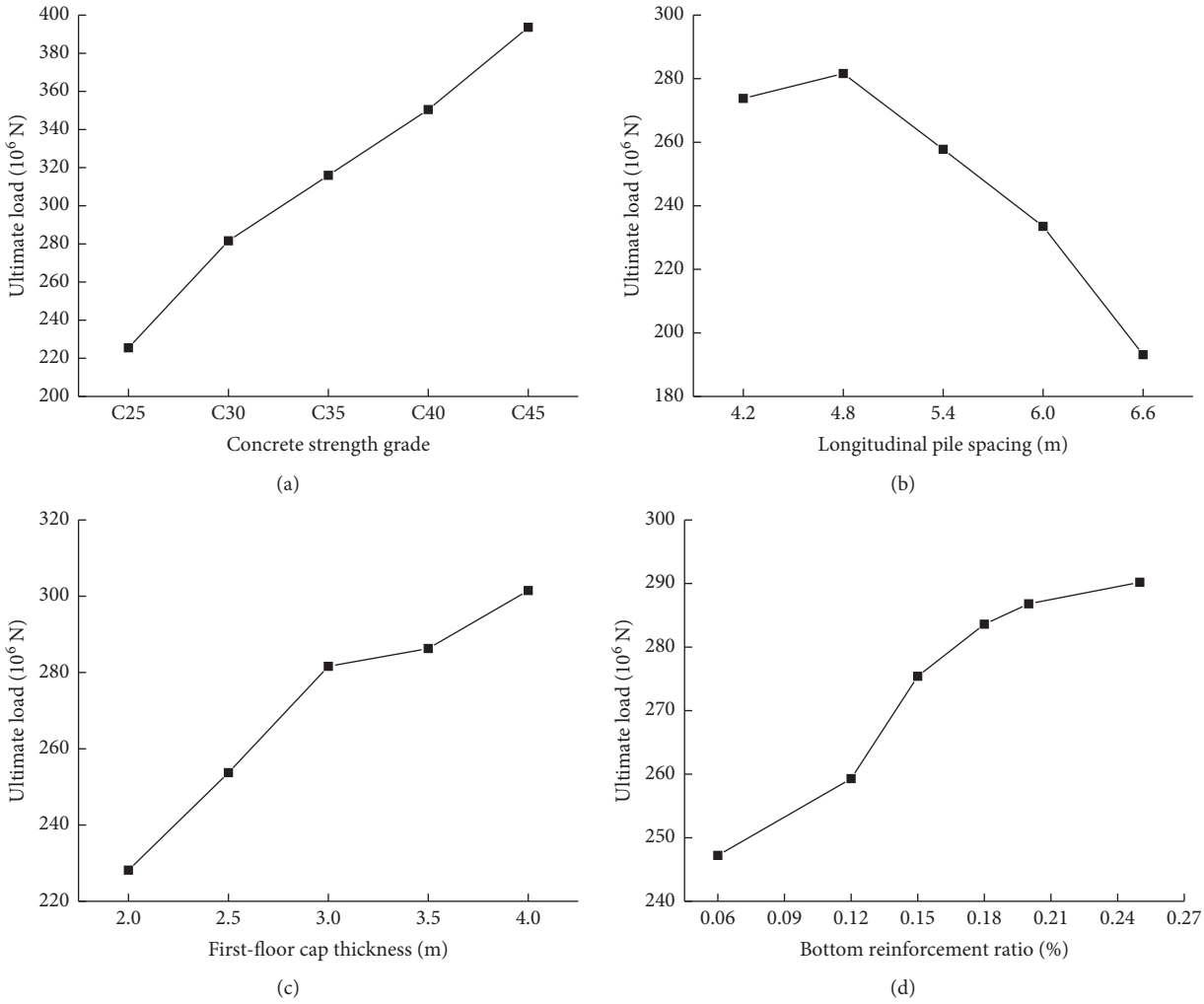

Figure 4: Influencing curve of vertical ultimate load at cap top with parameter variation of different influencing factors. (a) Concrete strength grade. (b) Pile spacing. (c) Cap thickness. (d) Reinforcement ratio.

Table 2: Vertical ultimate load at cap top with different reinforcement ratios and reinforcement distributed forms.

Reinforcement distributed form	Uniform reinforcement						Concentrated reinforcement	
Reinforcement ratio (%)	0.06	0.12	0.15	0.18	0.20	0.25	0.12	0.15
Ultimate load (10^6 N)	247.2	259.3	275.4	283.6	286.8	290.2	283.4	287.1

When $\alpha \geq 45^\circ$ [see Figure 5(d)], cracks first appeared around the edge pile, began to appear around the middle pile with increasing load, and developed obliquely upward. Meanwhile, bending cracks appeared at the midspan between piles at cap bottom and expanded upward. After intersecting with oblique cracks on the edge pile, cracks continued to expand upward. When cracks extended to cap top, cap was declared to be damaged, showing bending failure.

3.3. Reaction Force at Pile Top. Since the structure and load were symmetrical, the reaction forces at No. 1 to No. 3 and No. 6 to No. 8 pile top within 1/4 cap were extracted; therein, No. 1 pile was corner pile, No. 8 pile was middle pile, and the rest were edge piles [see Figure 1(a)].

Reaction forces at pile top in this study were consistent with results of spatial truss model test and numerical simulation presented by He et al. [23]. As can be seen from Figure 6 and Table 3, the reaction force at each pile top under vertical load was not equal; the middle pile top had the highest value, followed by edge pile top and corner pile top. As α increased, the proportion of reaction force decreased at corner pile, No. 2 edge pile, and No. 3 edge pile, while that proportion increased at the middle pile, No. 6 edge pile, and No. 7 edge pile. Under ultimate load, the maximum pile reaction force at $\alpha = 52^\circ$ and $\alpha = 27^\circ$ was 1.97- and 1.4-fold

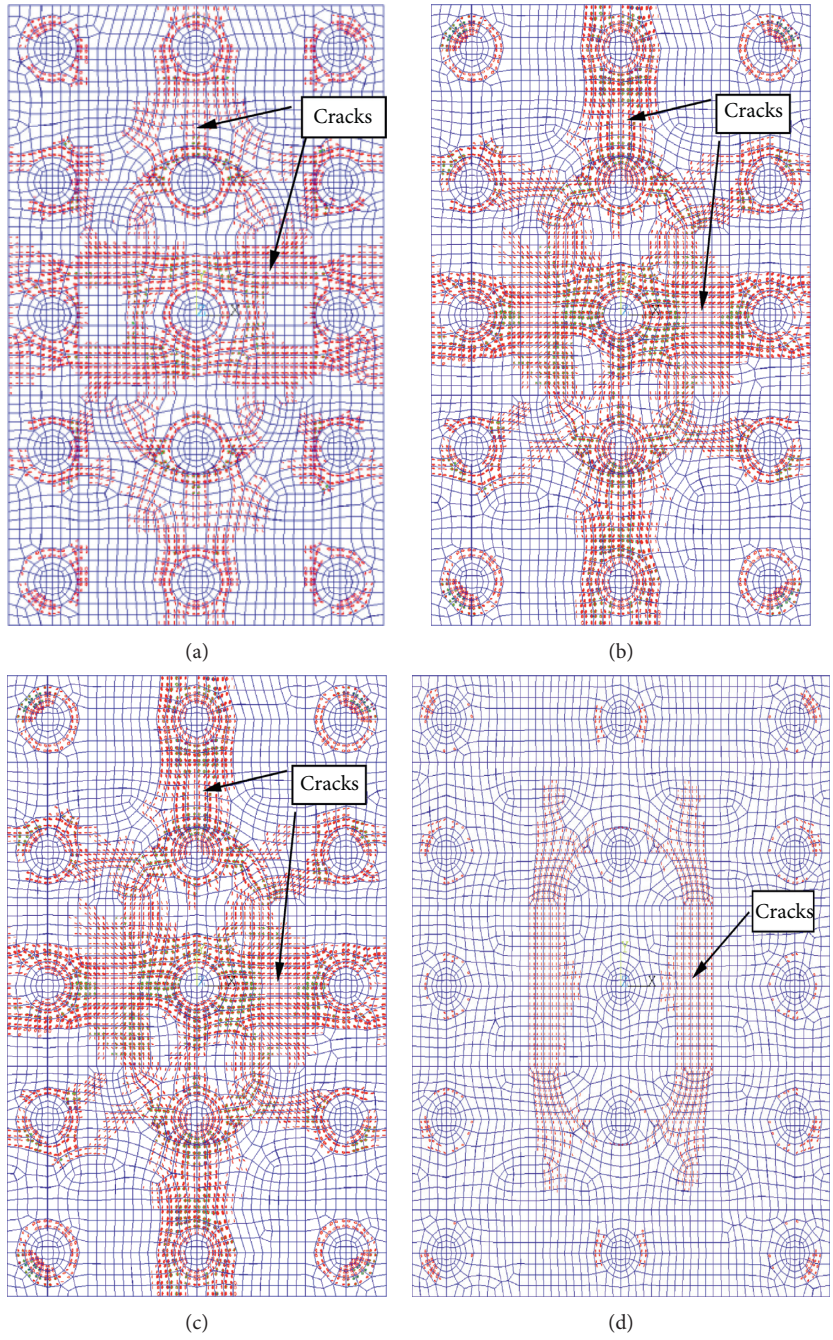

Figure 5: Cracks distribution varying with α. (a) $\alpha = 26^{\circ}$. (b) $\alpha = 34^{\circ}$. (c) $\alpha = 41^{\circ}$. (d) $\alpha = 52^{\circ}$.

greater than the minimum pile reaction force, respectively. The reaction force at pile top was closer when α was smaller, but the cap was not absolutely rigid. When α was larger, the punching was more serious. Under the action of load, the capacity of load transferred to corner pile was weakened with the generation of damage inside the cap. As a result, corner pile could not continue to bear the load, and the load was transferred to the middle pile, which caused middle pile failure in advance. Therefore, middle pile should be considered strengthening in cap design.

3.4. Stress Trajectory. Figures 7(a) and 7(c) show the distribution of elastic principal compressive stresses in the concrete under vertical load and combined load (horizontal force, vertical force, and bending moment), respectively. The principal compressive stresses were mainly transmitted along the line between the pile and the outer edge of pier, while the stress trajectories in other areas were less distributed. Concrete in this area provided cap structure safety. The first-floor cap top and the pile top experienced a state of three-way compression. Figures 7(b) and 7(d) show the distribution of elastic principal tensile

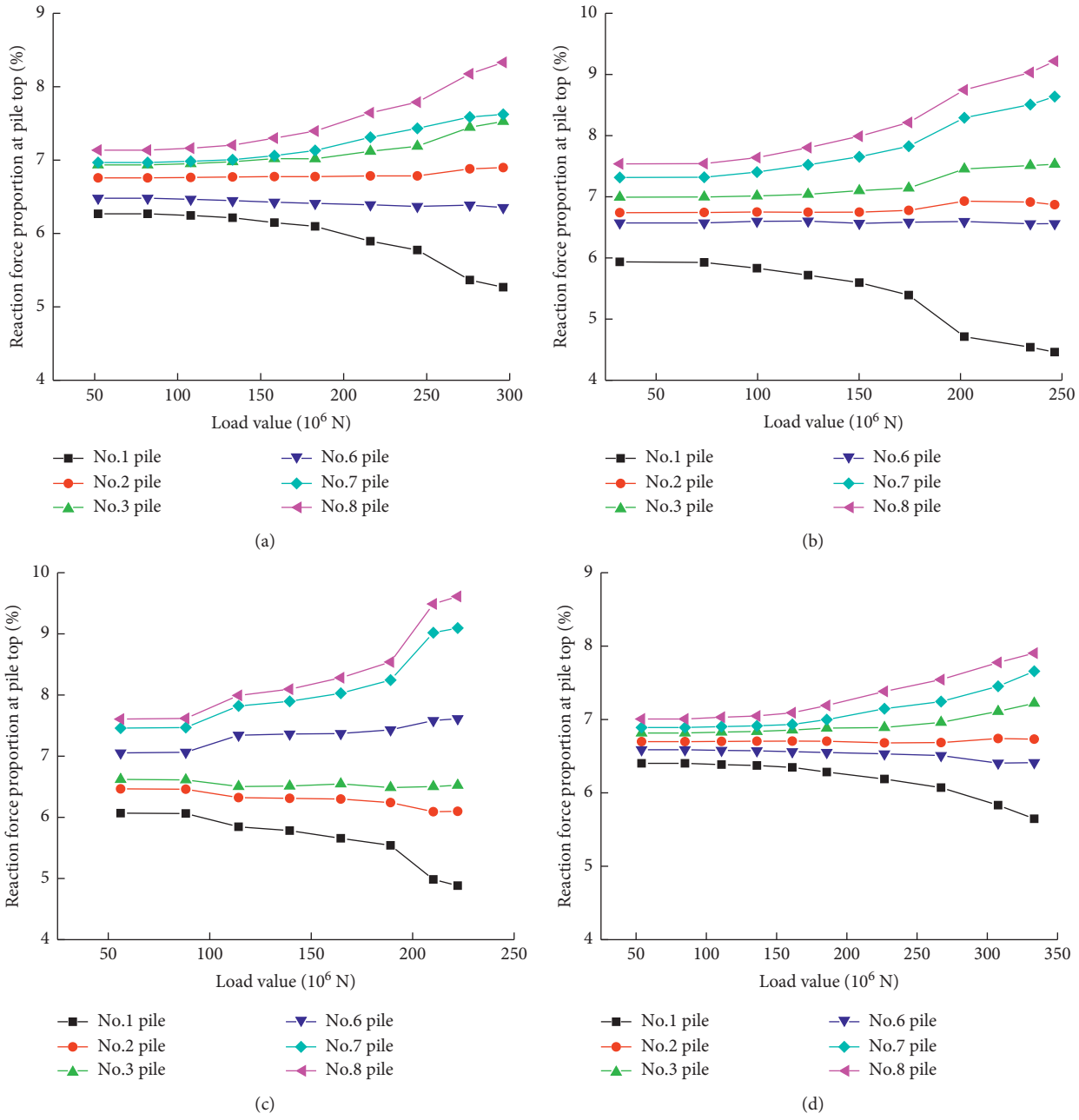

Figure 6: Curve of the reaction force proportion at pile top with vertical load when α changes. (a) $\alpha = 26^\circ$. (b) $\alpha = 52^\circ$. (c) $\alpha = 46^\circ$. (d) $\alpha = 27^\circ$.

stresses in the concrete under vertical load and the combined load, respectively. Concrete at a certain height at cap bottom was under tension which was borne by steel bars.

3.5. Steel Bar Stress Distribution. Figure 8 shows the stress distribution curve of horizontal steel bars at cap bottom. The maximum stress of steel bars was distributed between pile and pile connection. After cracking of concrete at cap bottom, the effective range of reinforcement effect was roughly within the pile diameter range, and the stresses of steel bars at other positions were relatively small. The steel bars within the pile diameter range between pile and pile connection served as tie bars.

4. Calculation Method for Bearing Capacity of Tie and Strut

The failure mechanism, elastic principal stress trajectories in the concrete, and stresses distribution in the reinforcement were summarized as follows. According to the development of cracks inside the cap, cracked reinforced concrete carried load principally by compressive stresses in the concrete and

Table 3: Reaction force at each pile top under ultimate load (including self-weight loads) (unit: 10^6 N).

Calculated parameters		Ultimate load	The reaction force at pile top					
			No. 1 pile	No. 2 pile	No. 3 pile	No. 6 pile	No. 7 pile	No. 8 pile
Cap thickness	2.0 m ($\alpha = 46^\circ$)	246.4	11.0	16.9	18.6	16.2	21.3	22.7
	2.5 m ($\alpha = 39^\circ$)	272.8	13.6	18.0	20.7	17.9	22.5	24.2
	3.0 m ($\alpha = 34^\circ$)	306.4	14.8	18.0	19.4	17.4	20.8	21.8
	3.5 m ($\alpha = 30^\circ$)	312.2	16.6	21.3	23.0	20.2	24.4	25.6
	4.0 m ($\alpha = 27^\circ$)	333.4	18.8	22.4	24.1	21.4	25.5	26.4
Pile spacing	4.2 m ($\alpha = 26^\circ$)	296.1	15.6	20.4	22.3	18.8	22.6	24.7
	5.4 m ($\alpha = 41^\circ$)	284.3	14.5	18.4	20.2	20	23.7	25.2
	6.0 m ($\alpha = 47^\circ$)	260.8	13.1	16.5	17.8	19	22.6	23.8
	6.6 m ($\alpha = 52^\circ$)	222.2	10.9	13.6	14.5	16.9	20.2	21.4

Note. When cap thickness = 3.0 m, the corresponding pile spacing = 4.8 m. To avoid repetition, results for pile spacing = 4.8 m are not presented in Table 3.

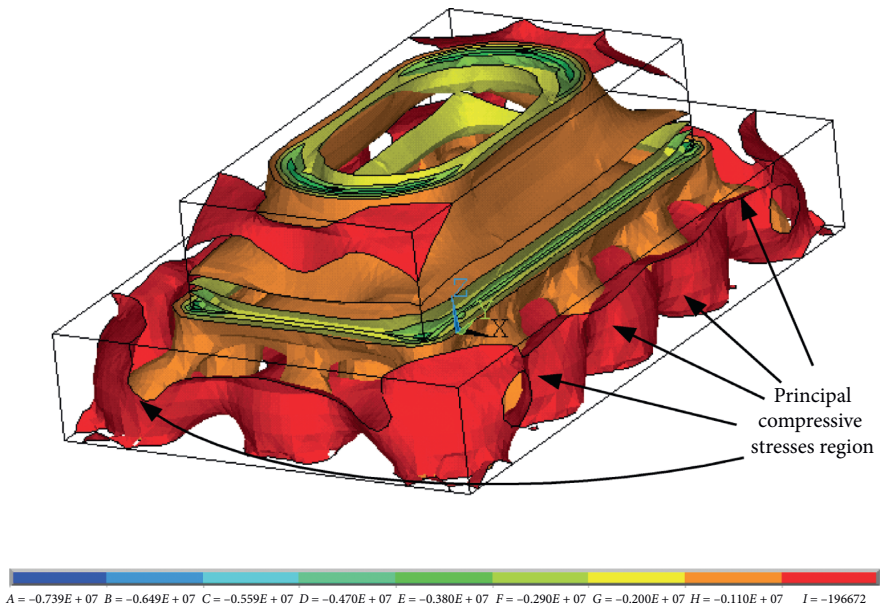

(a)

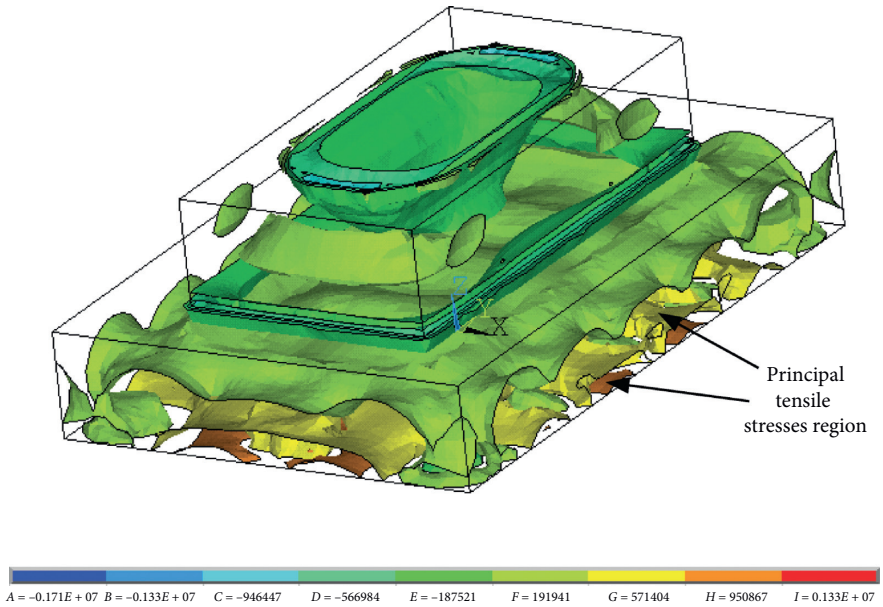

(b)

Figure 7: Continued.

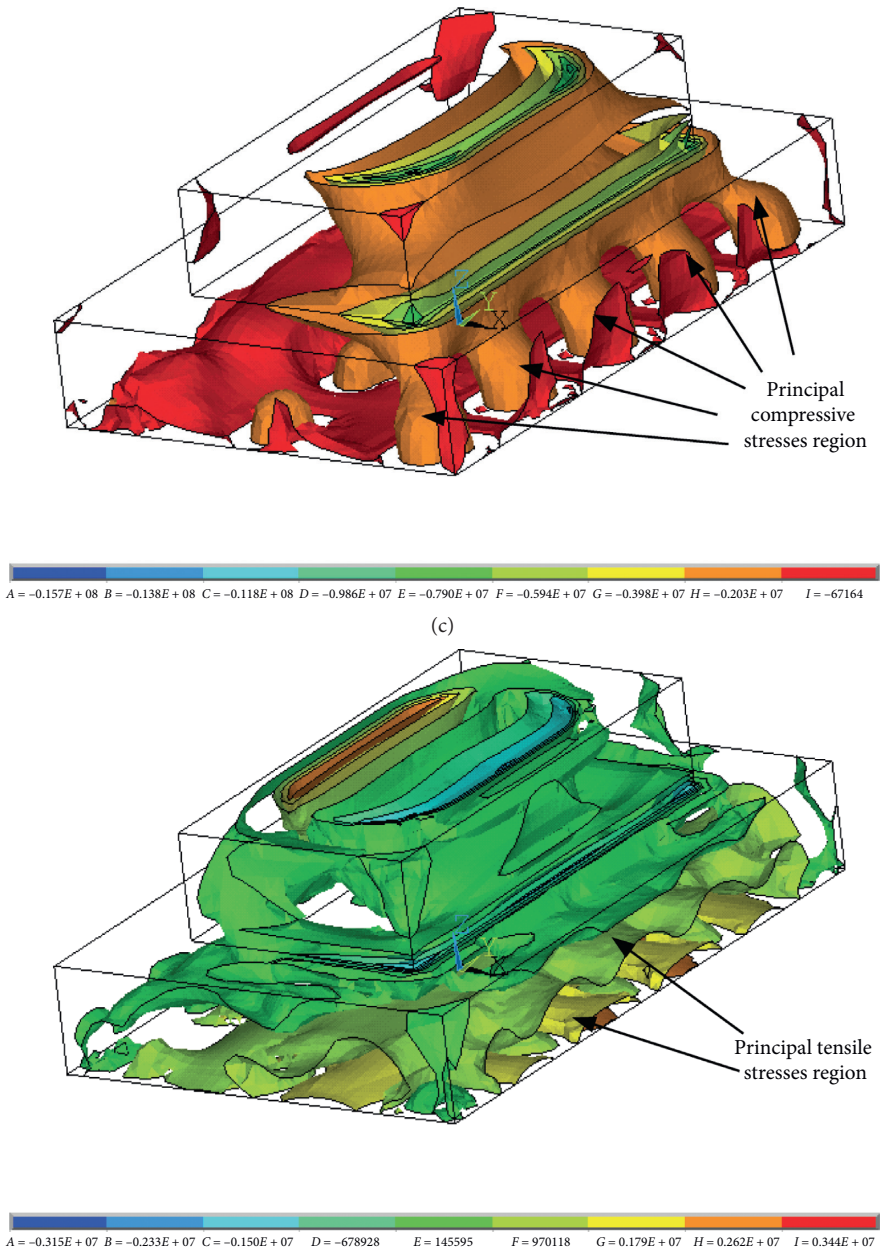

FIGURE 7: Isosurface of principal stresses distribution under vertical load or combined load. (a) Principal compressive stresses under vertical load. (b) Principal tensile stresses under vertical load. (c) Principal compressive stresses under combined load. (d) Principal tensile stresses under combined load.

tensile stresses in the reinforcement. The mechanical characteristic of railway cap conforms to the simplified calculation model of the spatial truss, in which concrete lying between pier outer edge and piles inside cap serves as struts, the steel bars at cap bottom within the pile diameter range are tie bars, the junction surface at cap top serves as the top node, and the junction points between struts and tie bars serve as the bottom node. From isosurface of elastic principal compressive stress trajectories in the concrete, it can be seen that concrete struts intersected at a surface but not a point under vertical load, which is similar to the composite spatial truss model. Under combined load with a large proportion of bending moment, mechanical characteristics of cap conform to the ordinary spatial truss model. The simplified spatial truss model under different loads is shown in Figure 9.

According to STM and the calculation method of strut and tie in CAN/CSA S6-14, JTG 3362-2018, and AASHTO LRFD-2017, based on the mechanical behavior and failure mechanism of railway cap, and code for design of concrete structures of railway bridge and culvert using the allowable stress method, the calculation method for the design of

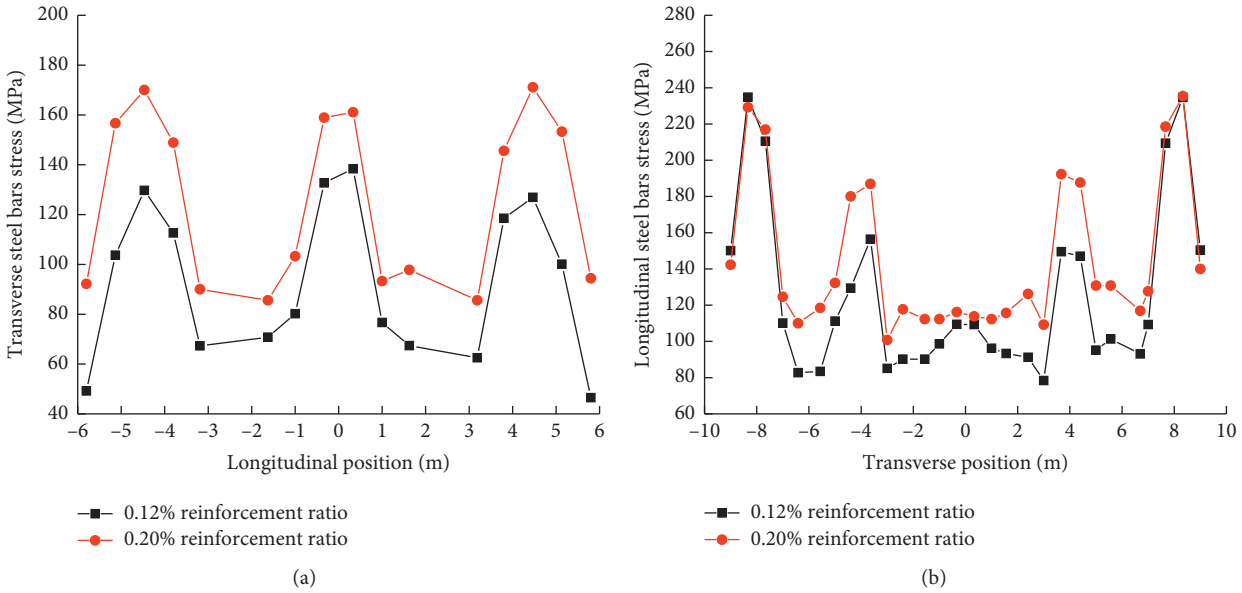

Figure 8: Stress values and distribution of steel bars. (a) Transverse steel bars along the longitudinal position. (b) Longitudinal steel bars along the transverse position.

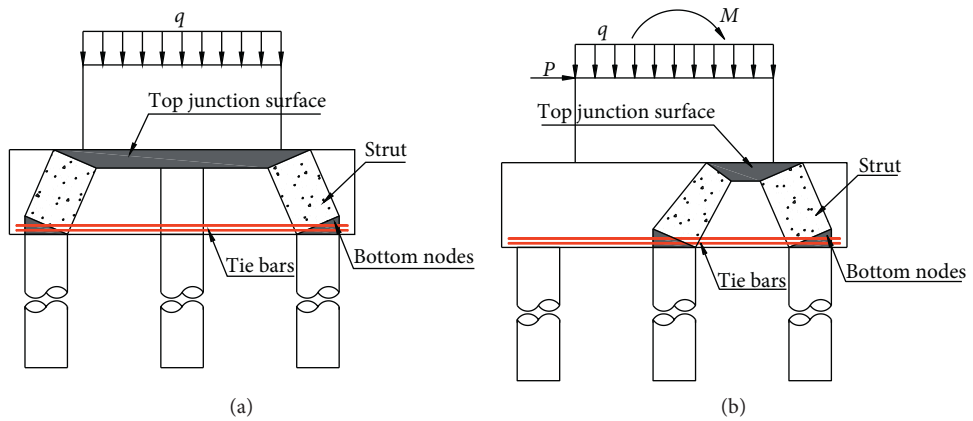

Figure 9: Construction of the spatial truss model under different loads. (a) Vertical load. (b) Combined load.

railway cap is recommended with considering the strength safety factors of the material [24].

4.1. Reaction Force Calculation at Pile Top. Reaction forces at pile top under vertical load are not equal; i.e., the cap is not absolutely rigid. Checking calculation of bearing capacity using formulas for rigid cap produces certain blindness, which may cause potential safety hazards to practical engineering applications. The pile reaction force is related to cap rigid angle, load transfer path, geological conditions, load forms on cap top, piles arrangement, and the shearing effects of soil between piles.

FEM can be used to calculate accurate reaction force at pile top of railway caps by establishing pile cap model based on the linear elastic assumption. The spring stiffness coefficient calculated by "m" method is applied to the nodes of piles model to simulate the pile foundation constraint. The tie bar force in the spatial truss model is calculated according to the static equilibrium by the maximum reaction force at pile top in the same row piles. The strut force is the larger value of the result according to the static equilibrium by maximum reaction force at pile top in the same row piles and the reaction force at middle pile top.

4.2. Bearing Capacity of Tie Bar. We found that the effective stresses of longitudinal steel bars mainly concentrated within pile diameter by analyzing the reinforcement stresses distribution under different reinforcement ratios. Considering the strength safety factor, the allowable stress value of steel bar was determined [24], and the bearing capacity of tie bar should be

$$T \le A_s[\sigma_s], \tag{1}$$

where T is the design value of the tie bar force under load, which is calculated according to the static equilibrium of

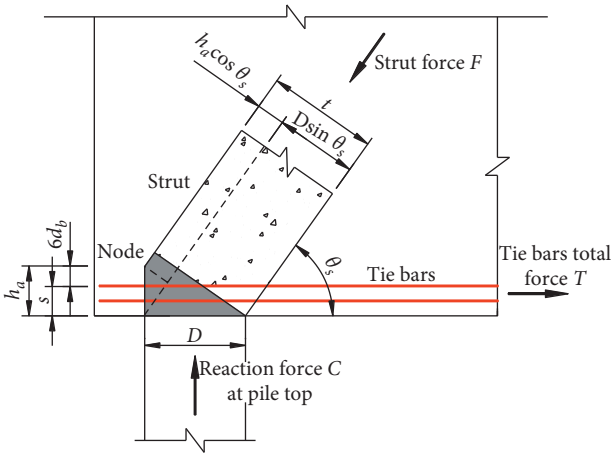

Figure 10: Schematic diagram of calculation size of strut.

Table 4: Comparison of ultimate load of caps between FEM and the present method.

Calculation model		Ultimate load		(2)/(1)[a]
		(1) The result of FEM (10^6 N)	(2) The result of present method (10^6 N)	
Concrete strength grade	C25	249.5	238.8	0.957
	C30	306.4	280.9	0.917
	C35	340.0	330.1	0.971
	C40	374.5	379.2	1.013
	C45	417.7	421.4	1.009
Pile spacing (m)	4.2	296.1	303.1	1.024
	5.4	284.3	257.0	0.904
	6.0	260.8	234.7	0.900
	6.6	222.2	215.2	0.968
Cap thickness (m)	2.0	246.4	223.6	0.907
	2.5	272.8	257.2	0.943
	3.5	312.2	298.7	0.957
	4.0	333.4	311.4	0.934
The average value of the ratio is 0.954 with a variance of 0.042				

Note. The calculation model of cap thickness = 3.0 m and pile spacing = 4.8 m is the same as that of concrete strength grade C30; therefore, not all of them are listed in Table 4. [a]Ratio of the result of present method (2) and FEM (1).

spatial truss model; A_s is the total area of longitudinal steel bars within pile diameter at cap bottom; and $[\sigma_s]$ is the allowable stress value of steel bar.

4.3. Bearing Capacity of Strut. The bearing capacity of concrete strut was checked according to the following formula:

$$F \le A_c[\sigma_c], \tag{2}$$

where F is the design value of strut force under load, which is calculated according to the static equilibrium of spatial truss model; A_c is the effective area of concrete strut; and $[\sigma_c]$ is the allowable stress value of concrete.

According to principal compressive stress trajectories, the cross section of strut is elliptic and the strut is a cylinder. Strut section height (presented in Figure 10) was calculated according to (3) and (4), referring to the provisions in AASHTO LRFD.

$$t = D\sin\theta_s + h_a\cos\theta_s, \tag{3}$$

$$h_a = s + 6d_b, \tag{4}$$

where t is the calculated height of strut; D is the pile diameter; h_a is the length of the back face of a node; θ_s is the inclination degree of the strut; s is the distance between the steel bar center at the top layer and the cap bottom; and d_b is the steel bar diameter.

When deducing formula of calculating splitting bearing capacity, it is considered that the compressive stress diffusion angle is diffused according to the formula $\theta = \arctan(1/2)$. The centroid of the bottom compression area is at 1/2 of the effective height, so the dimension of strut perpendicular to tie bar is $D + 0.5h_a$. The calculation of strut height along tie bar cannot consider diffusion range due to the anchorage of steel bar; strut height can be calculated according to (3). Therefore, the cross-sectional area of strut in the cap is calculated as

$$A_c = \frac{\pi\left(D\sin\theta_s + h_a\cos\theta_s\right)\left(D + 0.5h_a\right)}{4}. \quad (5)$$

The concrete allowable stress of central compressive member is calculated according to the ultimate compressive strength f_c of concrete considering the strength safety factor. The concrete strut is a cylinder-like central compression member. It is necessary to convert ultimate compressive strength of concrete to that of a cylinder, to obtain the effective compressive strength of strut, i.e., the allowable stress of concrete strut.

The relationship between f_c and $f_{cu,k}$ is approximated as

$$f_c = 0.67 f_{cu,k}. \quad (6)$$

The relationship between $f_{cy,k}$ and $f_{cu,k}$ is approximated as

$$f_{cy,k} = 0.8 f_{cu,k}. \quad (7)$$

According to (6) and (7), the relationship between $f_{cy,k}$ and f_c is as follows:

$$f_{cy,k} = 1.2 f_c. \quad (8)$$

With a 2.5 safety coefficient of central compressive member, the allowable stress of concrete strut is calculated as follows:

$$[\sigma_c] = \beta\frac{1.2 f_c}{2.5} = 0.48\beta f_c, \quad (9)$$

where f_c is the ultimate compressive strength of concrete; $f_{cu,k}$ is the compressive strength standard value of 150 mm concrete cube; $f_{cy,k}$ is the compressive strength standard value of φ150 mm × 300 mm concrete cylinder; and β is the increase coefficient of allowable stress under different load combinations.

4.4. Validation of Calculation Method. The Results of the calculation method presented in this study were compared with FEM of different concrete strength grade, longitudinal pile spacing, and cap thickness values, as shown in Table 4. The average ratio of our values to that of FEM was 0.954 with a variance of 0.042, showing good agreement between them. Strength safety coefficient derived from our method is conservative, which is beneficial to the structure safety. Therefore, the calculation method this paper proposed can be used to calculate the ultimate load of cap and further to design and check the cap.

5. Conclusions

FEM was used to analyze the mechanical behavior for fifteen-pile thick cap of mixed passenger and freight railway bridge. Concrete strength grade, cap thickness, pile spacing, reinforcement ratio, and reinforcement distributed form directly affected bearing capacity of cap. The cap showed punching failure as $\alpha < 45°$. Reaction forces at pile top under vertical load were not equal; the force was larger at the middle pile top than that at the edge pile top and showed its minimum at the corner pile top, suggesting that the cap is not absolutely rigid. The principal compressive stress trajectories in the concrete were mainly transmitted along the line between pile and pier outer edge, while the effective stresses of reinforcement were mainly distributed in the pile diameter range between pile and pile connection.

According to the failure mechanism, principal stress trajectories in the concrete, and stresses distribution in the reinforcement, this paper proposed a spatial truss model which was applicable to the design of railway caps. The spatial truss model was composed of concrete struts and steel tie bars interconnected at nodes; concrete between pier outer edge and piles inside the cap served as struts, and the steel bars at cap bottom within the pile diameter range were tie bars. With reference to the relevant specifications of cap design, the formulas for calculating the bearing capacity of strut-and-tie bar were presented. A comparison between our results and that of FEM indicated that our method could be used to calculate the ultimate load of cap and further to design and check cap of railway bridge.

Data Availability

The data used to support the findings of this study are available from the corresponding author upon reasonable request.

Conflicts of Interest

The authors declare that there are no conflicts of interest regarding the publication of this paper.

Acknowledgments

This work was partly supported by the Fundamental Research Funds for the Central Universities (31920200059).

References

[1] H. L. Guo and B. Jiang, "Study of pile cap failure type discrimination," *Engineering Mechanics*, vol. 30, no. 6, pp. 142–147, 2013.

[2] R. Souza, D. Kuchma, J. W. Park, and T. Bittencourt, "Adaptable strut-and-tie model for design and verification of four-pile caps," *ACI Structural Journal*, vol. 106, no. 2, pp. 142–150, 2009.

[3] X. B. Huang, C. Y. Liu, S. Hou et al., "An analysis of the impact exerted on bearing capacity of pier and pile after increasing pile cap height," *Shock and Vibration*, vol. 2018, p. 9, 2018.

[4] A. G. Bloodworth, J. Cao, and M. Xu, "Numerical modeling of shear behavior of reinforced concrete pile caps," *Journal of Structural Engineering*, vol. 138, no. 6, pp. 708–717, 2012.

[5] M. Victoria, O. M. Querin, and P. Martí, "Generation of strut-and-tie models by topology design using different material properties in tension and compression," *Structural and Multidisciplinary Optimization*, vol. 44, no. 2, pp. 247–258, 2011.

[6] P. Chetchotisak and J. Teerawong, "Reliability-based assessment of RC pile cap design methods and proposals for their strength resistance factors," *KSCE Journal of Civil Engineering*, vol. 23, no. 8, pp. 3372–3382, 2019.

[7] ACI, Building Code Requirements for Structural Concrete and Commentary, American Concrete Institute,Farmington Hills, MI, USA, 2014.

[8] British Standards Institution. *Structural Use of Concrete, Part 1: Code of Practice for Design and Construction*, British Standards Institution, London, UK, 1997.
[9] K. S. Abdul-Razzaq and M. A. Farhood, "Design-oriented testing and modeling of reinforced concrete pile caps," *KSCE Journal of Civil Engineering*, vol. 23, no. 8, pp. 3509–3524, 2019.
[10] J. Park, D. Kuchma, and R. Souza, "Strength predictions of pile caps by a strut-and-tie model approach," *Canadian Journal of Civil Engineering*, vol. 35, no. 12, pp. 1399–1413, 2008.
[11] H. L. Guo, "Spacial strut and tie model for punching load transfer mechanism analysis of pile-cap," *Journal of Building Structures*, vol. 30, no. 1, pp. 147–156, 2009, in Chinese.
[12] C. F. Sun, Q. Gu, and S. M. Peng, "Experimental research on steel fiber reinforced concrete two-pile thick caps," *Journal of Building Structures*, vol. 31, no. 2, pp. 117–124, 2010, in Chinese.
[13] Y. M. Yun and J. A. Ramirez, "Strength of concrete struts in three-dimensional strut-tie models," *Journal of Structural Engineering*, vol. 142, no. 11, 2016.
[14] Y. Zhou and G.-L. Dai, "Parameter study of a new strut-and-tie model for a thick cap with six piles," *International Journal of Geomechanics*, vol. 16, no. 1, 2016.
[15] C. E. Broms, "Strut-and-tie model for punching failure of column footings and pile caps," *ACI Structural Journal*, vol. 115, no. 3, pp. 689–698, 2018.
[16] Y. M. Yun, B. Kim, and J. A. Ramirez, "Three-dimensional grid strut-and-tie model approach in structural concrete design," *Aci Structural Journal*, vol. 115, no. 1, pp. 15–26, 2018.
[17] CSA Group, *Canadian Highway Bridge Design Code*, Canadian Standards Association, Mississauga, Canada, 2016.
[18] China Communications Press, *Specifications for Design of Highway Reinforced Concrete and Prestressed Concrete Bridges and Culverts*, China Communications Press Co., Ltd, Beijing, China, 2018.
[19] American Association of State Highway and Transportation Officials, *Bridge Design Specifications*, American Association of State Highway and Transportation Officials, Washington, DC, USA, 8 edition, 2017.
[20] China Railway Publishing House, *Code for Design on Subsoil and Foundation of Railway Bridge and Culvert*, China Railway Publishing House Co., Ltd, Beijing, China, 2017.
[21] China Architecture and Building Press, *Code For Design of Concrete Structures (The 2015 Version)*, China Architecture and Building Press, Beijing, China, 2015.
[22] H. B. Wang, Z. S. Xu, and W. X. Ren, "Analysis of natural frequency about 3-dimensional pile group-pile cap-pier," *Journal of Changsha Railway University*, vol. 17, no. 2, pp. 74–79, 1999.
[23] H. N. He, G. L. Dai, and Y. L. Diao, "Spatial truss model test and numerical simulation on thick caps of large-scale group piled foundation," *China Civil Engineering Journal*, vol. 48, no. 8, pp. 102–109, 2015.
[24] China Railway Publishing House, *Code for Design of Concrete Structures of Railway Bridge and Culvert*, China Railway Publishing House Co., Ltd, Beijing, China, 2017.